



ELSEVIER

Physics of the Earth and Planetary Interiors 119 (2000) 37–56

PHYSICS
OF THE EARTH
AND PLANETARY
INTERIORS

www.elsevier.com/locate/pepi

Seismic waveform modeling and surface wave tomography in a three-dimensional Earth: asymptotic and non-asymptotic approaches

Éric Clévedé^{a,*}, Charles Mégnin^b, Barbara Romanowicz^b, Philippe Lognonné^{a,c}

^a *Département de Sismologie, Institut de Physique du Globe de Paris, 4, Place Jussieu, case 89, 75252 Paris cedex 05, France*

^b *UC Berkeley Seismological Laboratory, 475 Mc Cone Hall, Berkeley, CA 94720-4760, USA*

^c *Département des études Spatiales, Institut de Physique du Globe de Paris, 4, Avenue de Neptune, 94107 Saint-Maur des Fossés cedex, France*

Received 1 March 1999; received in revised form 9 September 1999; accepted 10 September 1999

Abstract

We investigate the impact of the theoretical limitations brought by asymptotic methods on upper-mantle tomographic models deduced from long-period surface wave data (period > 80 s), by performing a synthetic test using a non-asymptotic formalism. This methodology incorporates the effects of back and multiple forward scattering on the wave field by summing normal modes computed to third order of perturbations directly in the 3D Earth, and models the sensitivity to scatterers away from the great-circle path. We first compare the methods we used for the forward problem, both theoretically and numerically. Then we present results from the computation of 7849 synthetic Love waveforms in an upper mantle model consisting of two heterogeneities with power up to spherical harmonic degree 12. The waveforms are subsequently inverted using a 0th order asymptotic formalism (equivalent to a path-average approximation in the surface waves domain). We show that the main structures are retrieved, but that the theoretical noise on the output model is of the same order as the noise due to the path-coverage and a priori constraints. © 2000 Elsevier Science B.V. All rights reserved.

Keywords: Asymptotic; Non-asymptotic; 3D Earth

1. Introduction

Since the early 1980s global seismic tomography has provided images of the large scale variation of seismic velocities in the mantle (Woodhouse and Dziewonski, 1984). Tomographic models are widely

used to infer thermal and mineralogic heterogeneities in the mantle, making tomography a popular and powerful tool. The images of the uppermost mantle rely essentially on the inversion of surface wave data, as the body waves give poor resolution in this part of the mantle, due to the uneven distribution of seismic sources and receivers. All the global tomographic models seem to agree reasonably well on the long wavelength structure (i.e., the first 12 degrees in spherical harmonics, corresponding to a resolution

* Corresponding author. Fax: +33-1-44-27-38-94; e-mail: clevede@ipgp.jussieu.fr

of about 1500 km at the surface) between 100 and 600 km depth: the upper mantle is usually considered to be well resolved at the global scale (Dziewonski, 1995; Ritzwoller and Lavelly, 1995).

The tomographic process can be decomposed into three elements: the data selection, the inversion scheme and the underlying theory. Concerning the first point, tomographers have now access to an abundant supply of high quality digital data (e.g., from the GEOSCOPE and IRIS networks), ensuring that the coverage does not introduce significant bias in the inversion (at least for global surface wave data). The algorithms used to perform the inversion assume that the problem is quasi-linear, which, in the case of the large scale structure of the mantle is considered to be a robust hypothesis. If the data coverage and the inversion algorithms differ from one group to another, the theories employed to model the surface wave seismograms are very similar. Hence, the differences between the upper mantle tomographic models do not depend on the theory. The impact of the theory on the models obtained has never been fully assessed: the resolution tests performed use the same theory to compute synthetic data, giving only information on the quality of the data coverage, the selection scheme and the choice of a priori conditions.

The theory used for surface wave inversion in global tomography finds its formulation and first applications in the late 1970s and early 1980s (Jordan, 1978; Woodhouse and Girnius, 1982; Woodhouse, 1983; Tanimoto, 1984; Woodhouse and Dziewonski, 1984). It relies on two assumptions: the lateral variation of the seismic velocities are small in amplitude (a few percent with respect to a global average), and vary smoothly (the lateral velocity gradients are small). This implies in theoretical terms that the actual wave field in the mantle is a weak perturbation with respect to a spherically symmetric Earth, and that the wave propagation is well explained by the laws of geometrical optics. In other words, the wave equation in the Earth is simplified by two approximations: the first order Born approximation (the heterogeneities are considered as secondary sources in an unperturbed reference wave field), and the 0th-order asymptotic approximation (or high frequency approximation: the wave number of the seismic signal is higher than the wave number of the

anomalies, so the wave path can be modeled by a 0-dimension ray laterally). These approximations were necessary for computational purposes, as a global inversion of surface wave data requires the computation of several thousands of seismograms and their partial derivatives with respect to the seismic parameters, which is still a huge task in terms of computation time and size of the problem.

In the past 10 years, numerous efforts have been directed towards improving the theoretical framework of surface wave propagation in a three-dimensional Earth (e.g., Woodhouse and Wong, 1986; Dahlen, 1987; Park, 1987; Romanowicz, 1987; Snieder and Nolet, 1987; Snieder and Romanowicz, 1988; Lognonné and Romanowicz, 1990; Park, 1990; Lognonné, 1991; Tromp and Dahlen, 1992; Friederich et al., 1993; Tromp and Dahlen, 1993; Pollitz, 1994; Wang and Dahlen, 1994; Cummins et al., 1997). However, most global tomography applications assume that the first-order Born approximation is valid and, in general, in its 0th-order asymptotic approximation. Most efforts beyond that have so far focused on regional applications, in studies of crustal and lithospheric structure (e.g., Alsina and Snieder, 1996; Alsina et al., 1996; Meier et al., 1997a,b; Friederich, 1998), where lateral variations are known to be large and strong effects on waveforms have been documented.

Only one attempt has been made to introduce more accurate waveform modeling in global mantle imaging: Hara et al. (1993) used a non-asymptotic fully-coupled modes method (Geller and Hara, 1993; Geller et al., 1990) to infer S-wave velocity in the upper mantle in a long wavelength (degree-8 laterally) model, and compared a posteriori the results with the M84A model (Woodhouse and Dziewonski, 1984). Even at this large scale they found significantly different results. However, no one has ever tried to estimate experimentally the theoretical noise in the inversion scheme and the resulting models.

In this paper we try to test the theoretical noise induced by using first order Born and asymptotic approximations in global upper mantle tomography using long-period surface wave data. To do so, we compute long-period seismic waveforms using the method developed by and Lognonné (1991) and Lognonné and Romanowicz (1990) (hereby referred as HOPT, for Higher Order Perturbation Theory)

where normal modes of a given aspherical model are computed using HOPT, and where no asymptotic approximation is assumed.

In Sections 2 and 3 we recall the main features of the methods used in this paper. Section 4 addresses the theoretical differences between these methods. In Section 5 we introduce our test model and compare synthetic seismograms and phase velocity observations. Section 6 presents the inversion of the synthetic data, computed with the HOPT method, using first order Born and asymptotic approximations. The number of seismograms and the coverage are realistic, corresponding to the surface waveform data used in the whole mantle shear velocity model SAW12D by Li and Romanowicz (1996) consisting in 7849 SH accelerograms of first and second orbit Love waves.

2. Asymptotic theory

In this paper K will denote a normal mode multiplet (corresponding to a doublet (n, l)) consisting of $2l + 1$ normal mode singlets k (triplet (n, l, m)), with l the angular order, n its radial order, and m its azimuthal order. The superscript (0) will refer to a spherical reference Earth model, the superscript (n) (with $n > 0$) will refer to an order of approximation of the actual Earth. The equation defining the displacement field $u(x, t)$ due to an earthquake can be written (in the non-rotating case):

$$(A + K\partial_t^2)u(x, t) = f(x, t), \quad (1)$$

where A is the elasto-dynamic operator, $K(x)$ is the density distribution and $f(x, t)$ is the equivalent body force distribution of the source. In the case of a step function source where $\partial_t f_i(t) = \delta(t)S_i$, the corresponding accelerogram is (exactly):

$$s(t) = \Re e [\text{Rexp}(iHt) K^{-1}S], \quad (2)$$

where R is the receiver term, S the source term, K is the density term and H is defined by the relation: $H^2 = K^{-1}A$. Lets consider the normal modes of a spherical non-rotating elastic isotropic Earth model (SNREI) $|u_k\rangle$, which verify the homogeneous eigenvalue equation is:

$$(A^{(0)} - K^{(0)}w_k^2)|u_k\rangle = 0, \quad (3)$$

where $w_k = w_K$, ($k \in K$) is the eigenvalue and $|u_k\rangle$ the eigenfunction of the singlet k of the degenerated multiplet K . They obey the orthogonality conditions:

$$K_{kk'}^{(0)} = \langle v_{k'} | K^{(0)} | u_k \rangle = \delta_{kk'}, \quad (4)$$

$$A_{kk'}^{(0)} = \langle v_{k'} | A^{(0)} | u_k \rangle = w_K^2 \delta_{kk'}, \quad (5)$$

$$H_{kk'}^{(0)} = \langle v_{k'} | H^{(0)} | u_k \rangle = w_K \delta_{kk'}, \quad (6)$$

Following Woodhouse (1983), the operators representing the laterally heterogeneous Earth are decomposed as the sum of a reference spherical term and a first order aspherical perturbation term: $\Theta^{(1)} = \Theta^{(0)} + \delta_1 \Theta$ with $\Theta_{kk'}^{(0)} \gg \delta_1 \Theta_{kk'}$, where Θ can assume the values of K , A and H , and with (Woodhouse, 1983; Li and Tanimoto, 1993):

$$\langle v_{k'} | K^{(1)-1} | u_k \rangle = \delta_{kk'} - \langle v_{k'} | \delta_1 K | u_k \rangle, \quad (7)$$

and

$$\begin{aligned} \langle v_{k'} | H^{(1)} | u_k \rangle \\ = w_K \delta_{kk'} + \frac{\langle v_{k'} | \delta_1 H | u_k \rangle - w_K^2 \langle v_{k'} | \delta_1 K | u_k \rangle}{w_K + w_{K'}}, \end{aligned} \quad (8)$$

or equivalently (Li and Romanowicz, 1995):

$$\begin{aligned} \langle v_{k'} | H^{(1)} | u_k \rangle \\ = (w_K + \delta w_K) \delta_{kk'} \\ + \frac{\langle v_{k'} | \delta_1 H | u_k \rangle - w_K^2 \langle v_{k'} | \delta_1 K | u_k \rangle - 2w_K \delta w_K \delta_{kk'}}{w_k + w_{k'}}, \end{aligned} \quad (9)$$

where

$$\delta w_K = \frac{\sum_{k, k' \in K} \langle R | u_{k'} \rangle \langle v_{k'} | \delta_1 H | u_k \rangle \langle v_k | S \rangle}{\sum_{k \in K} \langle R | u_{k'} \rangle \langle v_k | S \rangle}, \quad (10)$$

is the location parameter defined by Jordan (1978), corresponding to an apparent frequency shift of a multiplet for a given seismogram.

Eq. (2) can be written, neglecting the amplitude term due to the density perturbation (e.g., Woodhouse, 1980; Romanowicz, 1987; Li and Tanimoto, 1993):

$$s(t) = \Re e [\text{Rexp}(iHt) S]. \quad (11)$$

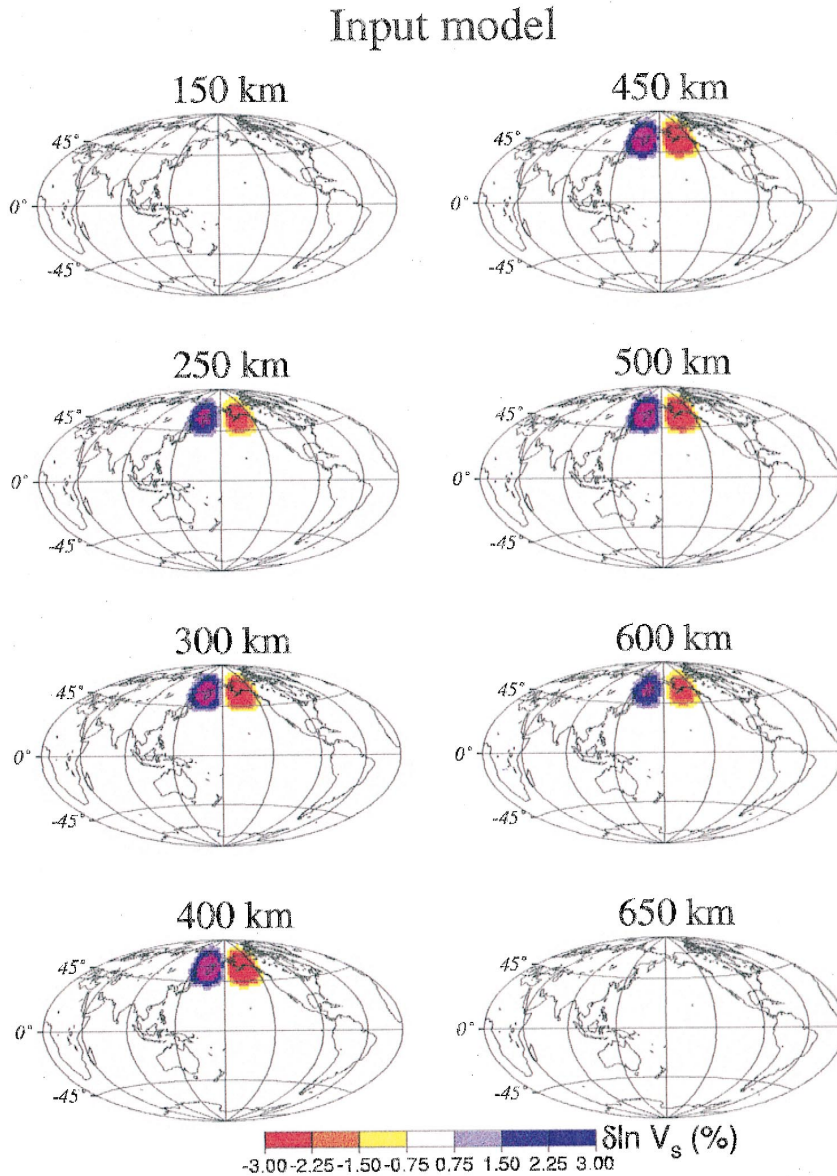


Fig. 1. Input model: the heterogeneities are located in the upper mantle and expanded up to spherical harmonic degree 12 laterally and 5th order Legendre polynomials radially (see Fig. 2). The small structures around the main heterogeneities are due to the spherical harmonic truncation.

Following Woodhouse (1983), and choosing the approximation (9), the phase term can be linearized:

$$\exp(iH_{kk'}^{(1)}t)$$

$$= \exp(i\hat{w}_K t) \delta_{kk'}$$

$$+ (\delta_1 H_{kk'} - w_{K'}^2 \delta_1 K_{kk'} - 2w_K \delta w_K \delta_{kk'})$$

$$\times \frac{\exp(i\hat{w}_K t) - \exp(i\hat{w}_{K'} t)}{(w_K + w_{K'}) (\hat{w}_K - \hat{w}_{K'})}$$

$$- i\delta w_K \exp(i\hat{w}_K t), \quad (12)$$

Input model

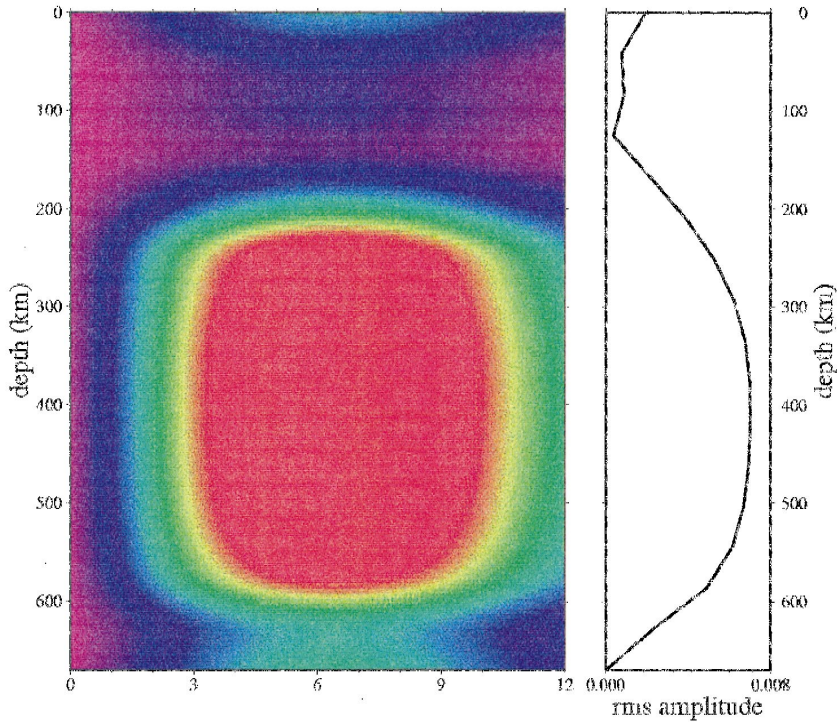


Fig. 2. Spectral content and rms profile of the input model. The left plot shows the amplitude spectrum (spherical harmonic degrees in abscissa) at each depth in the upper mantle.

where $\hat{w}_K = w_K + \delta w_K$ and $w_{K'} = \hat{w}_{K'} + \delta w_{K'}$. Using the equality (12) in Eq. (11) results in the expression of the first order Born approximation seismogram obtained by Li and Romanowicz (1995). If the approximation (8) is chosen, we obtain the expression of Li and Tanimoto (1993).

At this point, we assume that the spatial wavelengths of the structure are much larger than the seismic wavelengths considered. Under this high frequency hypothesis, it is possible to estimate asymptotically the phase and amplitude perturbations: when $s_{\max} \ll \min(l)$, s_{\max} being the maximum angular order of the model expressed in spherical harmonics and l the angular order of any mode considered (e.g., Romanowicz and Roul, 1986), we can use the following approximation:

$$Z_{mm'}^{Kk'} = 2w_{kk'} \int_{\Omega} \delta w_{kk'}(\theta, \phi) Y_l^{m*}(\theta, \phi) \times Y_l^m(\theta, \phi) d\Omega, \quad (13)$$

with m and m' referring to the azimuthal order of the singlets $k \in K$ and $k' \in K'$, respectively, and where the Y_l^m are the fully normalized spherical harmonics (Edmonds, 1960), and the scattering term can then be written (see Li and Tanimoto, 1993, for the definition of each terms):

$$\begin{aligned} & \sum_{mm'} R_m^k Z_{mm'}^{k'k'} S_{m'}^{k'k'} \\ &= \left(\frac{(2l+1)}{4\pi} \frac{(2l'+1)}{4\pi} \right)^{1/2} \sum_{NM} R_{kN} S_{k'M} \\ & \times \int_{\Omega} \delta w_{kk'}^2 P_l^N(\cos \theta_{pr}) P_{l'}^M(\cos \theta_{ps}) \\ & \times \exp[i(M\phi_{ps} - N\phi_{pr})] d\Omega_p. \end{aligned} \quad (14)$$

To order $1/l$, the associated Legendre function in Eq. (14) can be reduced to a cosine (e.g., Romanow-

icz, 1987). Applying the stationary phase to the two resulting integrals yield:

$$s(t) = s_{\text{PAVA}}(t) + s_1(t) + \sum_K \sum_{K' \in \Gamma_K} D_{KK'}(t) E_{KK'}, \quad (15)$$

where $s_{\text{PAVA}}(t)$, the ‘‘Path Average’’ seismogram (Jordan, 1978; Woodhouse and Dziewonski, 1984), is

$$s_{\text{PAVA}}(t) = \sum_K A_K \exp(i\hat{w}_K t) \text{ with} \\ A_K = \sum_{k \in K} \langle R|u_k \rangle \langle v_k|S \rangle, \quad (16)$$

and

$$s_1(t) = - \sum_K i t \delta \tilde{w}_K A_K \exp(i\hat{w}_K t). \quad (17)$$

Γ_K is the set of multiplets with eigenfrequencies $w_{K'} \geq w_K$ and the time dependent term is defined as:

$$D_{KK'}(t) = \frac{\exp(i\hat{w}_K t) - \exp(i\hat{w}_{K'} t)}{(w_K + w_{K'})(\hat{w}_K - \hat{w}_{K'})}, \quad (18)$$

and the asymptotic scattering terms $E_{KK'}$, where only the $\pi\phi$ dependent terms are kept inside the integral, are given in Li and Romanowicz (1995)(Eq. 12 and Appendix A).

3. Non-asymptotic theory

The non-asymptotic HOPT has been developed by Lognonné and Romanowicz (1990) and Lognonné (1991). Let us summarize the principal points of the method.

We start from the normal modes of a spherical non-rotating anelastic isotropic Earth model (SNRAI). The eigenmodes and eigenfrequencies of the three-dimensional Earth model are expressed using perturbation theory. The eigenmodes $|u_k\rangle$ and associated complex eigenfrequencies σ_k , with $\sigma_k = w_k + i\alpha_k$, are solutions of:

$$-\sigma_k^2 K|u_k\rangle + \sigma_k B|u_k\rangle + A(\sigma_k)|u_k\rangle = 0, \quad (19)$$

where A is the elasto-dynamic operator and B the Coriolis operator. Note that now the problem lies in

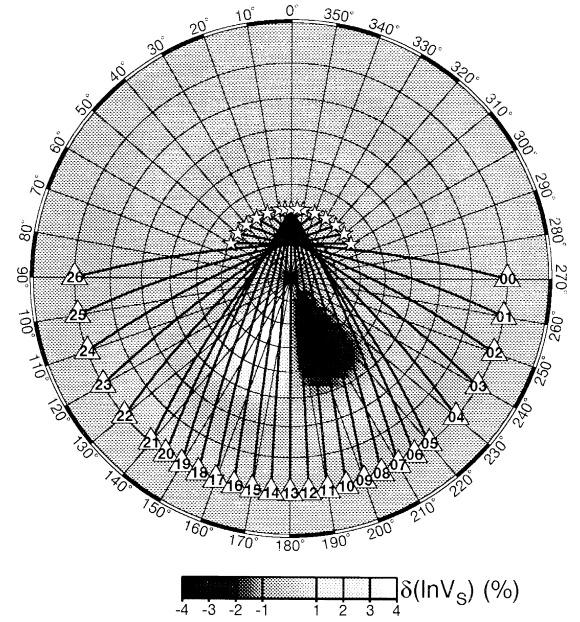


Fig. 3. Source–receiver paths used in the forward modeling experiment: the sources are represented by the stars and the receivers, labeled clockwise, by the triangles. The epicentral distance is 110° for all the paths.

the complex space. Here the model can include laterally heterogeneous anelastic and anisotropic structure.

Let us define the Hamiltonian H :

$$H^2 = K^{-1}(\sigma B + A(\sigma)). \quad (20)$$

The n th order approximation of the problem (Eq. (19)), in the sense of the perturbation theory, where $|u_k\rangle$ and σ_k are developed in terms of a power series of a small parameter ϵ related to the perturbation of the operator A , is:

$$\sigma_k^{(n)}|u_k^{(n)}\rangle = H^{(n)}|u_k^{(n)}\rangle + o(\epsilon^{(n+1)}), \quad (21)$$

To avoid a convergence problem occurring in the perturbation procedure due to the instability of the interaction terms within a multiplet, the perturbation path is constrained in order to cancel the first secular terms of the perturbation series. Then, $H^{(n)} = [H_{kk'}^{(n)}]$, with $H_{kk'}^{(n)} = \langle u_{k'}|H^{(n)}|u_k\rangle$, can be diagonalised such that:

$$H_{kk'}^{(n)} = \sigma_k^{(n+1)}\delta_{kk'} + o(\epsilon^{(n+1)}). \quad (22)$$

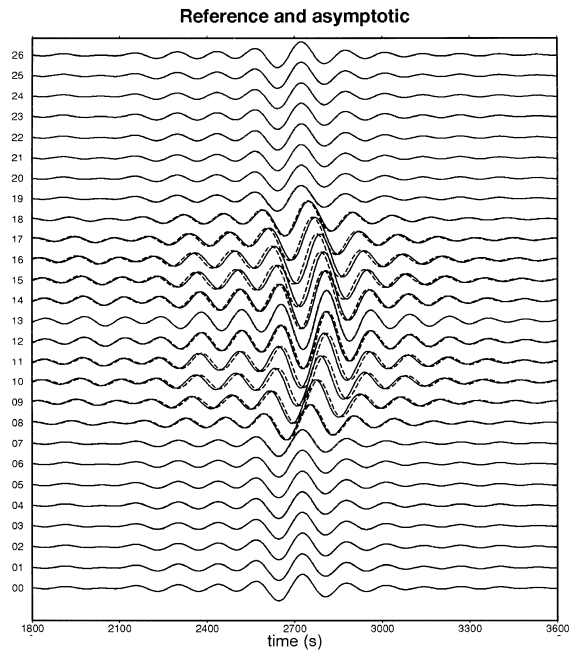


Fig. 4. Asymptotic (solid lines) and reference (dashed lines) seismograms. The seismograms are the transverse component with maximum frequency 8.0 mHz. The reference model is the spherically symmetric model PREM (Dziewonski and Anderson, 1981).

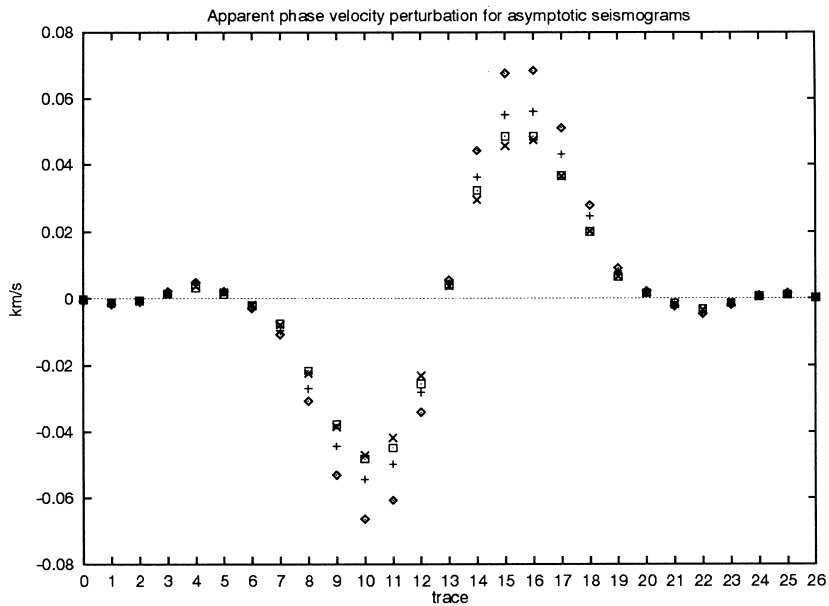


Fig. 5. Apparent phase velocity perturbation measured on the asymptotic seismograms represented on Fig. 4 at four different frequencies: 4 mHz (losanges), 5 mHz (pluses), 6 mHz (squares) and 7 mHz (crosses).

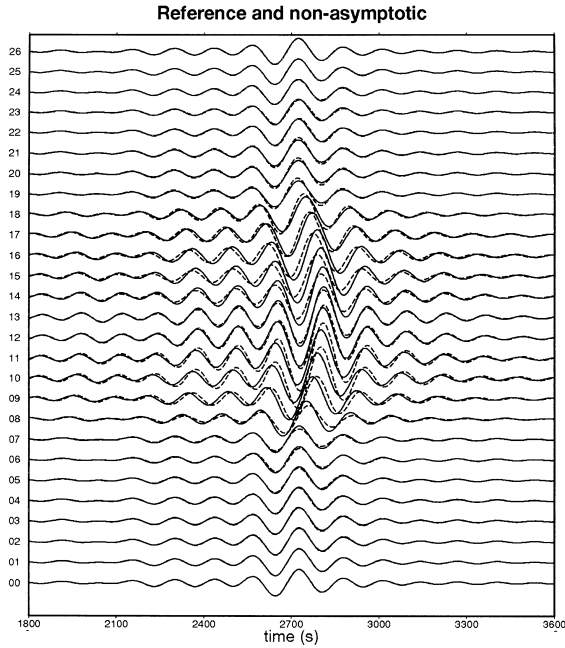


Fig. 6. Non-asymptotic (solid lines) and reference (dashed lines) seismograms.

A seismogram corresponding to a source $|S\rangle$ and a receiver $\langle R|$ will write as:

$$s^{(n)}(t) = \Re e \left[\sum_k \exp(it\sigma_k^{(n+1)}) \langle R|u_k^{(n)}\rangle \langle v_k^{(n)}|S\rangle \right] + o(t\epsilon^{(n+1)}), \quad (23)$$

$$s^{(n)}(t) = \Re e \left[\sum_K \exp(it\sigma_K^{(0)}) A_K^{(n)}(t) \right] + o(t\epsilon^{(n+1)}), \quad (24)$$

where σ_K^0 is the SNRAI complex frequency associated with the multiplet K , and the modulation function $A_K^{(n)}(t)$, a time-dependent function, which slowly modulates the oscillations of the spherical mode:

$$A_K^{(n)}(t) = \sum_{k \in K} \exp[it(\sigma_k^{(n+1)} - \sigma_K^{(0)})] \times \langle R|u_k^{(n)}\rangle \langle v_k^{(n)}|S\rangle. \quad (25)$$

In the absence of lateral heterogeneity, this function is constant in time, and simply represents the initial amplitude of the mode at the receiver.

The first order perturbation, in $t\epsilon$, corresponding to the 0th order in eigenfunction and first order in

eigenfrequency, is equivalent to the isolated multiplet hypothesis, for which only coupling between singlets in a same multiplet occurs, and this term is only sensitive to the symmetric part of the lateral heterogeneities. The higher order perturbations, in $t\epsilon^n$, correspond to the $(n-1)$ th order in eigenfunction and n th order in eigenfrequency, implying multiplet–multiplet coupling, and are both sensitive to symmetric and anti-symmetric lateral heterogeneities. A detailed analysis of the perturbation procedure is given by Lognonné (1991).

Lognonné and Romanowicz (1990) have shown that, in the elastic case (using the model M84, Woodhouse and Dziewonski, 1984), the second order approximation of the eigenmodes and third order of the eigenfrequencies compares with the solutions obtained with the variational method within a relative error lower than the observation error. We assume that in the following cases this order of perturbations is sufficient (the extension of the computation to higher orders is straightforward, but the gain in accuracy is outweighed by the computational cost).

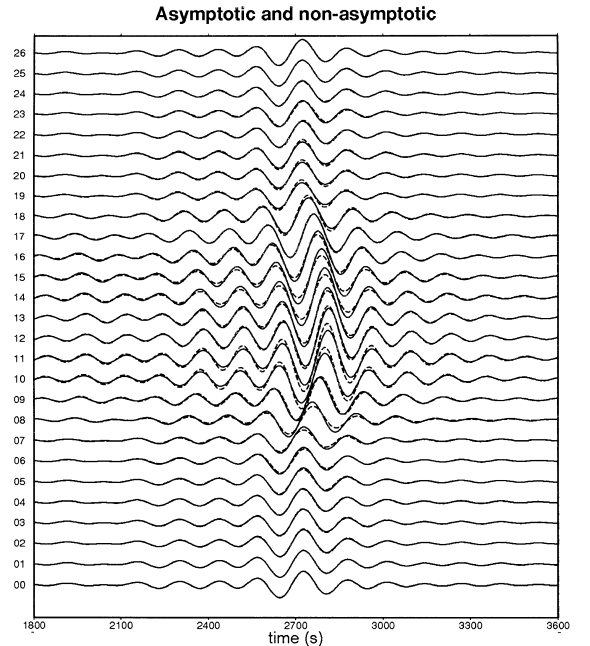


Fig. 7. Non-asymptotic (solid lines) and asymptotic (dashed lines) seismograms (see Figs. 4 and 6).

4. Theoretical comparison

As NACT and PAVA represent a first-order approximation in terms of the perturbation of the Hamiltonian H , a convenient way to relate HOPT to these methods is through the perturbation $\delta s(t)$ of the HOPT formulation of the seismograms, which corresponds to the first-order term of the Taylor expansion of the HOPT expression with respect to a perturbation of the structural parameters.

The derivatives appear through the expression:

$$s(t) \approx s_0(t) + \delta s(t)$$

where $s(t)$ is the synthetic seismogram in the perturbed model, $s_0(t)$ is the seismogram computed in the reference Earth model, and $\delta s(t)$ is the perturbation expressed in terms of the Fréchet derivatives. The estimation of $\delta s(t)$ in the general case, where the reference model is an a priori three-dimensional anelastic model, has been done by Clévéde and Lognonné (1996a). Considering the particular case of a spherical non-dispersive reference Earth model (and taking into account the problem of polarity rectified by Clévéde and Lognonné, 1996b), the expressions of the perturbation of the seismograms given by

Clévéde and Lognonné (1996a) (Eq. B4 and C1) reduces straightforwardly, as shown in Section A.1, to the short-time approximation given by Li and Tanimoto (1993) (Eq. 20):

$$s(t) = \Re e \left[\sum_K A_K(0) e^{i\sigma_K t} \right] + \Re e \left[\sum_K \sum_{K' \in \Gamma_K} \sum_{k \in K, k' \in K'} \frac{e^{i\sigma_{K'} t} - e^{i\sigma_K t}}{\sigma_K^2 - \sigma_{K'}^2} \times \langle R|u_k \rangle \langle v_k | \delta A | u_{k'} \rangle \langle v_{k'} | S \rangle \right], \quad (26)$$

where Γ_K is the set of multiplets whose eigenfrequencies $\sigma_{K'}$ are higher than or equal to σ_K . The first term in the right-hand side of Eq. (26) is the spherical contribution; the second term, corresponding to 3D structure effects, is valid for both self-coupling (i.e., within a multiplet: $K' = K$) and cross-coupling (i.e., between different multiplets: $K' \neq K$). If the coupling is restricted to modes that belong to the same dispersion branch, this expression is equivalent to the PAVA method before asymptotic approximation.

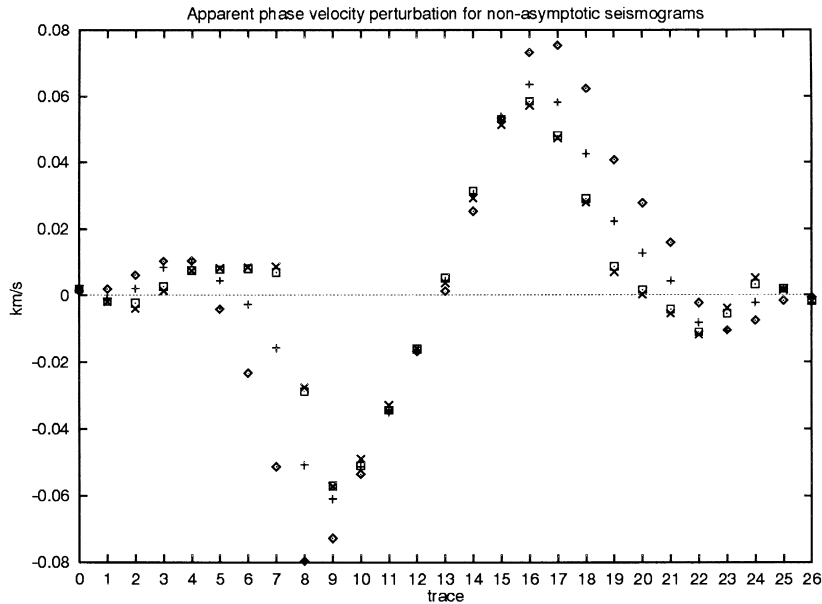


Fig. 8. Apparent phase velocity perturbation measured on the non-asymptotic seismograms represented on Fig. 6 at frequencies 4 mHz (losanges), 5 mHz (pluses), 6 mHz (squares) and 7 mHz (crosses).

In both cases no density perturbation is considered but, as shown by Lognonné and Romanowicz (1990), the density perturbation can be renormalized to yield a modified operator A . Perturbing the density with respect to the spherical density model then

produces a perturbation of the new operator A alone, thus the same formula applies.

Li and Romanowicz (1995) use a slightly different formulation by introducing the location parameter δw_K (expression 10), and by using the first order

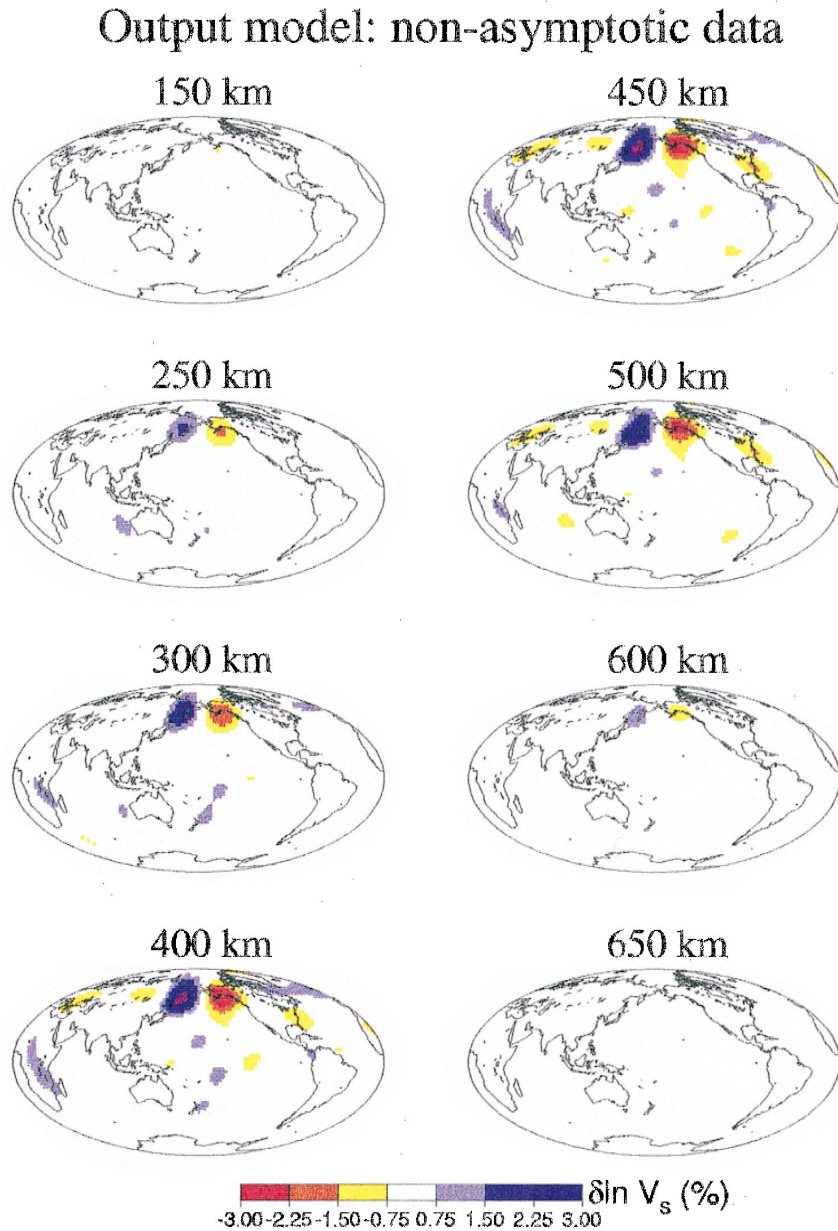


Fig. 9. Output model obtained using non-asymptotic data. These synthetic data are used as input in the inversion scheme based on the asymptotic assumption (“non-circular test”).

equivalence $1 + it\delta w_K \simeq e^{i\delta w_K t}$, which allows to remove the secularity arising in the self-coupling term. This corresponds, in terms of the modulation function, to approximating $A_K(t)$ by $A_K(0)e^{i\delta w_K t}$ (see also Woodhouse, 1983; Tanimoto, 1984). Using this approximation of the modulation function in the expression given by Clévéde and Lognonné (1996a), and keeping the first order terms in $\delta\sigma$, we obtain the following expression (see Section A.2):

$$\begin{aligned}
 s(t) = & \Re e \left[\sum_K A_K(0) e^{i\hat{\sigma}_K t} \right] \\
 & - \Re e \left[\sum_K it\delta w_K A_K(0) e^{i\hat{\sigma}_K t} \right] \\
 & + \Re e \left[\sum_K \sum_{K' \in \Gamma_K} \left(\frac{e^{i\hat{\sigma}_{K'} t} - e^{i\hat{\sigma}_K t}}{(\sigma_K + \sigma_{K'}) (\hat{\sigma}_K - \hat{\sigma}_{K'})} \right) \right. \\
 & \left. \times \sum_{k \in K, k' \in K'} \langle R|u_k \rangle \langle v_k | \delta A | u_{k'} \rangle \langle v_{k'} | S \rangle \right], \quad (27)
 \end{aligned}$$

where $\hat{\sigma}_K = \sigma_K + \delta w_K$. This formula is equivalent to the NACT expression of Li and Romanowicz (1995) (Eq. (15) in this paper). The first term is the non-linearized PAVA contribution. Note that in this case the normal modes are those of the spherical reference model. Thus, a first-order Born expansion of the HOPT seismogram reduces to a NACT seismogram.

A noticeable difference arises from the practical choice in the coupling between multiplets: on one hand, HOPT focuses on the coupling along the same dispersion branch (same radial order n , different

angular order l); on the other hand, NACT privileges coupling among different branches (different radial order n , same angular order l), while the coupling along the branch is treated asymptotically to the 0th order, as in the PAVA method: NACT is broad-band radially but assumes infinite frequencies laterally. In other words, NACT corresponds to “body-wave treatment” of the waveform (due to the choice of the coupling) with single scattering (due to the Born approximation), PAVA corresponds to “surface-wave treatment” with single scattering, while HOPT corresponds to “surface-wave treatment” with multiple scattering (as the actual wave field is computed — in the limit of the accuracy of the perturbation scheme). In the rest of this paper we perform numerical comparisons between the methods on long-period seismograms, involving only surface waves, for which NACT and PAVA are equivalent to the first order. Hence we expect the differences to mostly reflect the effect of finite frequencies versus infinite frequency approximation through lateral sensitivity to the structure.

Note that, despite the similarity with PAVA in the surface wave domain, we use NACT because the renormalization procedure applied on the modulation functions provides a better approximation with increasing time compared to the short-time approximation used in PAVA.

5. Numerical experiment: forward problem

As this paper focuses on the difference between asymptotic and non-asymptotic approaches, we need

Table 1

Maximum amplitudes at depth. The second column represents the maxima for the input model, the third column shows the maxima obtained by the inversion using asymptotic input data, the fourth column shows the maxima obtained by the inversion using non-asymptotic input data, and the fifth column the differences of the maxima depth by depth obtained by the two inversions

Depth (km)	Input model	Asymptotic data	Non-asymptotic data	Difference
150	−0.44%/0.45%	−1.55%/1.50%	−0.81%/0.77%	−0.76%/0.82%
250	−3.92%/3.98%	−3.39%/3.49%	−1.74%/1.76%	−1.76%/1.75%
300	−5.04%/5.12%	−4.13%/4.31%	−2.33%/2.44%	−1.91%/1.91%
400	−5.82%/5.91%	−4.92%/5.23%	−3.24%/3.56%	−1.88%/2.13%
450	−5.79%/5.88%	−4.89%/5.21%	−3.22%/3.59%	−1.88%/2.19%
500	−5.61%/5.70%	−4.55%/4.83%	−2.77%/3.14%	−1.96%/2.24%
600	−3.64%/3.69%	−3.07%/3.16%	−0.97%/1.16%	−2.11%/2.16%
650	−0.15%/0.15%	−2.09%/2.08%	−0.24%/0.32%	−1.80%/1.87%

to design a test such that expressions (23) and (27) are both in their domain of validity, so that we can compare the resulting seismograms. This supposes a smooth test model, and “short-time” seismograms, which in this case consists in the first direct and indirect surface-wave trains. In order to perform a

detailed analysis of the seismograms, we choose to consider a very simple structure. The model we designed, consists of two adjacent anomalies, one negative and one positive, with respect to the spherically symmetric PREM model (Dziewonski and Anderson, 1981). The heterogeneities extend from 200

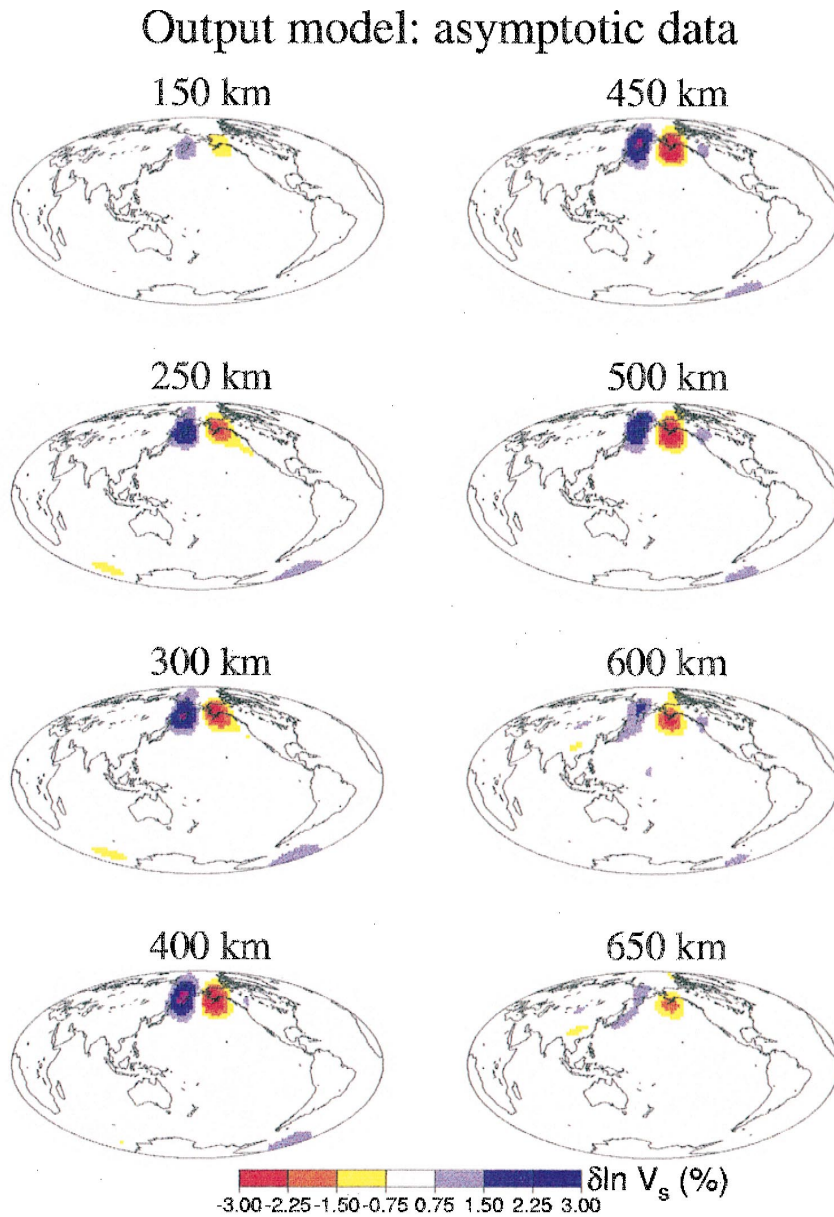


Fig. 10. Output model obtained using asymptotic data. These synthetic data are used as input in the inversion scheme based on the same asymptotic assumption (“circular test”).

to 600 km in depth, and 45° by 45° laterally. They are located between the North Pole and the latitude 45° North, hence the spectral content of the model is strong up to spherical harmonic degree 12. We expand the model in spherical harmonics up to the degree 12 laterally and radially to 5th order Legendre polynomials in the upper mantle (Figs. 1 and 2). The resulting model is used for both forward modeling and inverse problem tests.

All the seismograms presented in this section are on the transverse component and include all toroidal modes (fundamentals and harmonics) in the frequency band 0.3–8.0 mHz (3300–125 s). They are band-pass filtered with a cosine taper with corner frequencies 4.0 and 7.15 mHz (250–140 s). For all the seismograms the source is the same pure strike-slip at a depth of 33 km. The position of the sources and receivers is shown on Fig. 3. The epicentral distance varies between 106° and 110° , the 27 receivers (and traces) are labeled clockwise. As expected, for this particular window in the seismic signal NACT and PAVA give equivalent results (However, this is not true at significantly higher frequencies, as shown by Mégnin and Romanowicz, 1999a).

In the rest of this paper we will refer to NACT seismograms as asymptotic seismograms, because they are computed using the high frequency approximation described in Section 2, and to HOPT seismograms as non-asymptotic seismograms, because no approximation is done based on a relation between the wavelength of the structure and the seismic wavelength. For comparison we also computed the seismograms in the PREM model (Dziewonski and Anderson, 1981); these traces are referred as the reference seismograms in the text and figures.

We first make sure that the side lobes due to the truncation of the spherical harmonic expansion do not induce significant signal on the seismograms: paths far away from the main heterogeneities show variations of the order of 0.1%. However, the closest side-lobe, with a sign opposite to that of the heterogeneity, gives detectable signal and can be clearly identified, as we will see, on the phase velocity measurement obtained by cross-correlation with the reference seismograms for the wave packet associated to the fundamental branch (e.g., Suetsugu and Nakanishi, 1985).

Considering a clockwise sweep of the heterogeneities (Figs. 3 and 4), the asymptotic seismo-

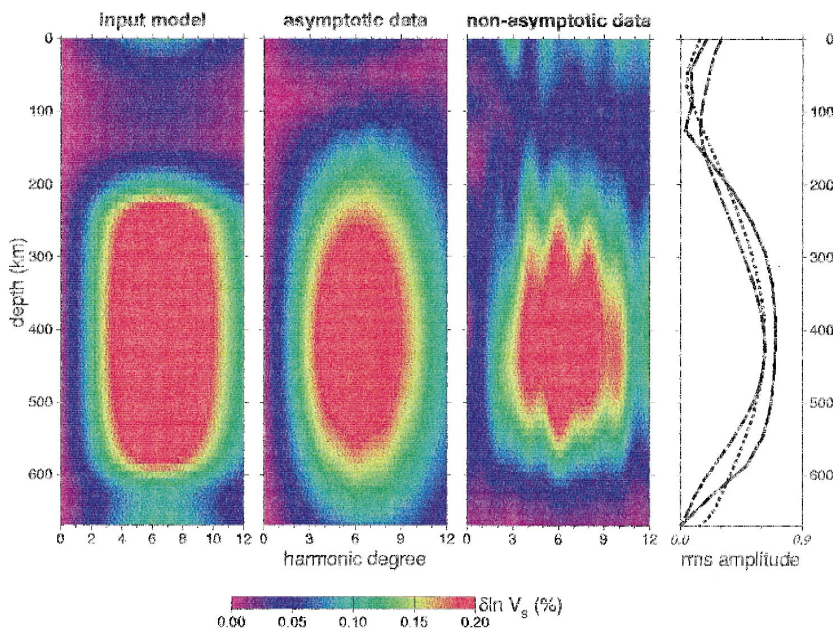


Fig. 11. Spectral contents and rms profiles of the output model obtained using asymptotic data (dotted line for rms) and non-asymptotic data (dashed line for rms), compared to the input model (solid line for rms). Conventions are the same as for Fig. 2.

grams start to record visible signal from the structure at station 07, located at longitude -155° , the signal disappearing after station 19 (longitude 155°). Note that for these seismograms, only the phase is perturbed. The apparent phase velocity perturbation, shown on Fig. 5, gives more precise information on the structure: the asymptotic approximation forces the same behavior for each frequency by collapsing the sensitivity to the structure on the great-circle path associated to the trace. The differences in amplitude reflect the location at depth of the heterogeneities. The location and relative strength of the structural side-lobes also appears (traces 03 to 05 and 21 to 23).

The corresponding results for the non-asymptotic seismograms (Fig. 6 for the comparison with the reference seismograms, and Fig. 7 for the comparison with the asymptotic seismograms) are shown in Fig. 8. The effect of the finiteness of the frequency manifesting itself through a Fresnel zone appears

clearly. The wavelength corresponding to the frequencies shown on Fig. 8 are about 1300 km at 4 mHz, 1000 km at 5 mHz, 825 km at 6 mHz and 685 km at 7 mHz. Due to the frequency dependence of the Fresnel zone width, the signal is difficult to interpret in the time domain, even for such a simple input model. For example traces 05 to 07 have evidently mixed information coming from both the main negative structure and the positive side-lobe. But it is also the case for all the traces at the lower frequencies, for which the Fresnel zone is wide enough to sample regions with a heterogeneity sign different from the one seen by the great-circle path.

6. Numerical experiment: inverse problem

Our goal in this study is to simulate realistic seismograms, in terms of the effects of the finiteness of the frequencies, by using a non-asymptotic ap-

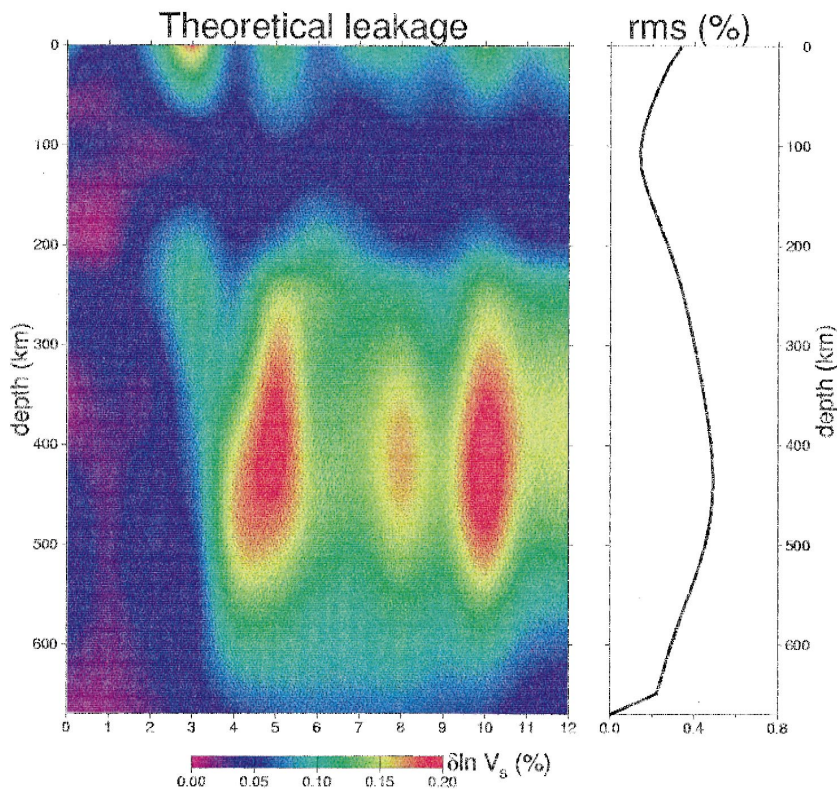


Fig. 12. Spectral content and rms profile of the difference between the asymptotic and non-asymptotic output models.

proach, and invert them with a quasi-standard asymptotic approach, in order to investigate the effects of using the asymptotic approach in real surface wave data inversion. We use our input model in the inversion procedure used by Li and Romanowicz (1996) based on the NACT method. Synthetic data are computed using the non-asymptotic HOPT method. The data set consists of 7849 seismograms corresponding to the actual surface-wave data coverage used in the SAW12D model (Li and Romanowicz, 1996), in the frequency window 2.5–12.5 mHz (400–80 s) band-passed with a cosine taper with corner frequencies 4–10 mHz (250–100 s), and time windows corresponding to Love waves trains G1 and G2 are selected.

In the inversion experiment we use the same synthetic pattern as in the forward problem: the scatterers represent less than 5% of the volume of the model. We made this choice, rather than using a global distribution of heterogeneities, in order to allow for most of the distortion effects to be actually seen as mapped heterogeneity.

Since we wish to isolate the effects of the distortion of the input structure due to the choice of the theoretical formalism from those of the subjective choice of a priori constraints, we compute the set of damping parameters that will minimize the Euclidian distance between input and output models. Using a simulated annealing algorithm coupled with a downhill simplex method (Press et al., 1992), we compute two optimal sets of damping parameters: one for the asymptotic data, one for the non-asymptotic data, which we use to regulate each of the two inversions.

The output model for the non-asymptotic input data is shown in Fig. 9. The main heterogeneities are retrieved, but spatially smeared. The maximum amplitudes at depth are given in Table 1. Spurious structure with maximum amplitude around 1% is found at every depth. However, these inaccuracies are a feature of the so-called “circular test” where the same theory is used in the forward modeling and inversion scheme. We performed such a test by using asymptotic input data generated with the NACT method. The same problems arise, but with much smaller effects on the model Fig. 10: the maximum amplitudes are well retrieved, and the heterogeneities are more localized, with a better contrast with the background velocities. These problems are, of course,

well known: the radial smearing can be partially attributed to the use of surface waves only; another factor contributing to the spatial smearing and underestimation of the real amplitudes is the use of damping parameters to stabilize the inversion procedure; errors in the estimation of the spherical harmonic coefficients cause global spurious structure. But the comparison between the models obtained in the “non-circular test” and the “circular test” shows that the theoretical noise is of the same order as the noise induced by the factors described above: off-path propagation effects contribute significantly to the surface waveform.

This can be clearly seen in the spectral domain. The spectral content of the models for the input model, the “non-circular test” and the “circular test” are shown on Fig. 11. Fig. 12 shows the spectral difference between the two output models. Both figures represent rms amplitude of the heterogeneity as a function of spherical harmonic degree (horizontal axis) and depth (vertical axis). The angular smearing appears clearly at all depths corresponding to the actual location of the input heterogeneities. Note that even if the fundamental surface wave energy is dominant in the data, part of the error can be attributed to the fact that overtone energy (wave trains X1 and X2), which is not treated the same way in NACT and HOPT (see Section 4), is present in some seismograms.

7. Conclusion

We have presented a comparison between long-period surface-wave synthetic seismograms computed with and without asymptotic approximation. Both forward modeling and upper-mantle tomography have been addressed.

We applied a standard surface-wave inversion procedure, built on the asymptotic approximation, using non-asymptotic waveforms as input data. The goal of this test is to assess the shortcomings of the asymptotic hypothesis in global mantle surface-wave tomography through an actual inversion. The output model shows that neglecting the lateral sensitivity of the surface waves to the structure leads to the underestimation of the amplitudes of the anomalies and to generation of spurious structure, adding a theoretical

factor to the numerical noise. We did not address the issue of noise in the data on purpose: adding noise to the synthetic data is, of course, a relevant test, but our goal is to isolate the problem of the choice of the theory.

This test is extreme for the asymptotic methods: only long-period surface-waves are involved, and the input model has a significant spectral content up to degree 12. We can still, of course, consider that the up-to-date tomographic models representing large spatial wavelengths of the upper mantle are reliable when considering the detection and location of the main structures, and the estimation of the characteristic parameters of the convection (Méglin et al., 1997; Méglin and Romanowicz, 1999b). The result of this test must be considered in the context of the many successes of asymptotic tomography. Increasing the spatial resolution of global mantle tomographic models using surface wave data faces serious theoretical problems. Park (1989) and Um et al. (1991) show that the asymptotic approximation breaks down rapidly for structure beyond angular degree 10, when using long-period surface wave data (period $T > 150$ s). This constitutes a hint that, even using shorter period data ($T > 80$ s), the presence of rough structures in the upper mantle (such as slabs and plumes) may introduce significant bias in an inversion scheme based on asymptotic approximations.

For the deeper mantle, on the other hand, where body waveform constraints are necessary to achieve any level of resolution, a more exact theoretical formalism such as HOPT is still computationally prohibitive. While computational enhancements are being sought for HOPT, asymptotic approximations such as NACT represent a significant theoretical improvement over PAVA, by allowing us to express the sensitivity of body waves to structure along the ray path more correctly (Li and Tanimoto, 1993; Li and Romanowicz, 1995; Méglin and Romanowicz, 1999a). An intermediate step beyond NACT, both for surface waves and for body waves, is to use higher order asymptotic approximations as described by Woodhouse and Wong (1986) and Romanowicz (1987). These methods asymptotically take into account the off-path influence of the structure on the signal. Although still limited by the high frequency approximation, this alternative should be considered

in the generation of long wavelength models, especially if we wish to retrieve information on anelasticity.

Acknowledgements

We thank Hendrik Jan van Heijst and anonymous reviewer for their comments and suggestions. We also thank Heiner Igel for his invitation to participate to this special issue, and Eléonore Stutzmann for providing us the phase velocity codes. This work was done during a post-doctoral position of EC at the UC Berkeley Seismological Laboratory. This is IGP contribution number 1659 and UC Berkeley Seismological Laboratory contribution number 99-07.

Appendix A

The perturbation of the seismogram with respect to a given reference model, in the non-dispersive case, is given by (Eq. B4 and C1 of Clévéde and Lognonné, 1996a,b):

$$\begin{aligned} \delta s_K(t) = & e^{i\sigma_K t} \left\{ \frac{i}{2\sigma_K} \int_0^t \langle R_K(t-\tau) | \delta A | S_K(\tau) \rangle d\tau \right. \\ & - \frac{1}{4\sigma_K^2} \int_0^t \langle \dot{R}_K(t-\tau) | \delta A | S_K(\tau) \rangle \\ & \left. + \langle R_K(t-\tau) | \delta A | \dot{S}_K(\tau) \rangle d\tau \right\} \\ & + \sum_{\substack{K' \neq K \\ \sigma_{K'} > K}} \left\{ \frac{e^{i\sigma_K t}}{\sigma_K^2 - \sigma_{K'}^2} \langle R_K(t) | \delta A | S_{K'}(0) \rangle \right. \\ & - \frac{e^{i\sigma_{K'} t}}{\sigma_K^2 - \sigma_{K'}^2} \langle R_K(0) | \delta A | S_{K'}(t) \rangle \\ & \left. + \frac{e^{i\sigma_K t}}{(\sigma_K^2 - \sigma_{K'}^2)^2} \right. \\ & \left. \times (2i\sigma_K \langle R_K(t) | \delta A | \dot{S}_{K'}(0) \rangle) \right\} \end{aligned}$$

$$\left. \begin{aligned} & -2i\sigma_{K'}\langle\dot{R}_K(t)|\delta A|S_{K'}(0)\rangle \\ & - \frac{e^{i\sigma_{K'}t}}{(\sigma_K^2 - \sigma_{K'}^2)^2} \\ & \times \left(2i\sigma_K\langle R_K(0)|\delta A|\dot{S}_{K'}(t)\rangle \right. \\ & \left. - 2i\sigma_{K'}\langle\dot{R}_K(0)|\delta A|\dot{S}_{K'}(t)\rangle \right) \end{aligned} \right\}. \quad (\text{A.1})$$

A.1. Spherical case

For a spherical reference model the modulation function is time-independent:

$$A_K(t) = \sum_{k \in K} \langle R|u_k\rangle\langle v_k|S\rangle = A_K(0), \quad (\text{A.2})$$

and so for the modulation fields at the receiver and the source:

$$\langle R_K(t)| = \langle R_K(0)| \quad (\text{A.3})$$

$$|S_K(t)\rangle = |S_K(0)\rangle. \quad (\text{A.4})$$

Replacing these fields in Eq. (A.1) gives:

$$\begin{aligned} \delta s_K(t) &= e^{i\sigma_K t} \frac{it}{2\sigma_K} \sum_{k, k' \in K} \langle R|u_k\rangle\langle v_{k'}|\delta A|u_k\rangle\langle v_k|S\rangle \\ &+ \sum_{\substack{K' \neq K \\ \sigma_{K'} > \sigma_K}} \frac{e^{i\sigma_{K'}t} - e^{i\sigma_K t}}{\sigma_K^2 - \sigma_{K'}^2} \\ &\times \sum_{\substack{k \in K \\ k' \in K'}} \langle R|u_k\rangle\langle v_k|\delta A|u_{k'}\rangle\langle v_{k'}|S\rangle. \end{aligned} \quad (\text{A.5})$$

Using

$$\lim_{\sigma_{K'} \rightarrow \sigma_K} \frac{e^{i\sigma_{K'}t} - e^{i\sigma_K t}}{\sigma_K^2 - \sigma_{K'}^2} = \frac{ite^{i\sigma_K t}}{2\sigma_K}, \quad (\text{A.6})$$

which means that Eq. C1 from Lognonné and Clévéde (1997) converges toward their Eq. B4 when $\sigma_{K'}$ converges toward σ_K . We obtain the following expression for the seismogram:

$$\begin{aligned} s(t) &= \sum_K A_K(0)e^{i\sigma_K t} + \sum_K \sum_{K' \in \Gamma_K} \frac{e^{i\sigma_{K'}t} - e^{i\sigma_K t}}{\sigma_K^2 - \sigma_{K'}^2} \\ &\times \sum_{\substack{k \in K \\ k' \in K'}} \langle R|u_k\rangle\langle v_k|\delta A|u_{k'}\rangle\langle v_{k'}|S\rangle, \end{aligned} \quad (\text{A.7})$$

with $\Gamma_K = \{K' | \sigma_{K'} \geq \sigma_K\}$. This equation is equivalent to the expression given by Li and Tanimoto (1993).

A.2. Spherical case with renormalisation of the modulation function

The location parameter, corresponding to the apparent frequency shift of an isolated multiplet, is defined by (Jordan, 1978):

$$\delta\sigma_K = \frac{\sum_{k, k' \in K} \langle R|u_k\rangle\langle v_k|\delta A|u_{k'}\rangle\langle v_{k'}|S\rangle}{2\sigma_K \sum_{k \in K} \langle R|u_k\rangle\langle v_k|S\rangle}. \quad (\text{A.8})$$

We renormalize the modulation function using this parameter:

$$A_K(t) = A_K(0)e^{i\delta\sigma_K t}, \quad (\text{A.9})$$

and the modulation fields at the source and the receiver become, along with their time derivatives:

$$\langle R_K(t)| = \langle R_K(0)|e^{i\delta\sigma_K t}$$

$$\langle\dot{R}_K(t)| = i\delta\sigma_K\langle R_K(0)|e^{i\delta\sigma_K t}, \quad (\text{A.10})$$

$$|S_K(t)\rangle = |S_K(0)\rangle e^{i\delta\sigma_K t}$$

$$|\dot{S}_K(t)\rangle = i\delta\sigma_K|S_K(0)\rangle e^{i\delta\sigma_K t}. \quad (\text{A.11})$$

Under the weak splitting hypothesis, we can write the following approximation:

$$\begin{aligned} \frac{1}{\sigma_k^2 - \sigma_{k'}^2} &\simeq \frac{1}{(\sigma_K + \sigma_{K'}) (\hat{\sigma}_K - \hat{\sigma}_{K'})} \\ &\times \left(1 - \frac{2(\hat{\sigma}_K - \delta\sigma_{K'})}{(\sigma_K + \sigma_{K'}) (\hat{\sigma}_K - \hat{\sigma}_{K'})} \delta\sigma_k \right. \\ &\left. + \frac{2(\hat{\sigma}_{K'} - \delta\sigma_K)}{(\sigma_K + \sigma_{K'}) (\hat{\sigma}_K - \hat{\sigma}_{K'})} \delta\sigma_{k'} \right), \end{aligned} \quad (\text{A.12})$$

where $\hat{\sigma}_K = \sigma_K + \delta\sigma_K$ and $\hat{\sigma}_{K'} = \sigma_{K'} + \delta\sigma_{K'}$, $\delta\sigma_k = \sigma_k - \sigma_K$ and $\delta\sigma_{k'} = \sigma_{k'} - \sigma_{K'}$ (with $k \in K$ and $k' \in K'$). Eq. (A.1) becomes:

$$\begin{aligned} \delta s_K(t) &= \frac{it}{2\sigma_K} e^{i\hat{\sigma}_K t} \left(1 - \frac{\delta\sigma_K}{2\sigma_K} \right) \sum_{k, k' \in K} \\ &\times \langle R|u_k\rangle\langle v_k|\delta A|u_{k'}\rangle\langle v_{k'}|S\rangle \\ &+ \sum_{\substack{K' \neq K \\ \sigma_{K'} > K}} \left\{ \frac{e^{i\hat{\sigma}_{K'} t} - e^{i\hat{\sigma}_K t}}{(\sigma_K + \sigma_{K'}) (\hat{\sigma}_K - \hat{\sigma}_{K'})} \right\}
 \end{aligned}$$

$$\times \left(1 + \frac{2(\hat{\sigma}_K \delta\sigma_K - \hat{\sigma}_{K'} \delta\sigma_{K'})}{(\sigma_K + \sigma_{K'}) (\hat{\sigma}_K - \hat{\sigma}_{K'})} \right) \times \sum_{\substack{k \in K \\ k' \in K'}} \langle R|u_k \rangle \langle v_k | \delta A | u_{k'} \rangle \langle v_{k'} | S \rangle \Bigg\}. \quad (\text{A.13})$$

As previously, we have the second term of Eq. (A.13) converging toward the first term when $\hat{\sigma}_{K'}$ converges toward $\hat{\sigma}_K$, and Eq. (A.13) can be written:

$$\delta s_K(t) = \sum_{K' \in \Gamma_K} \left\{ \frac{e^{i\hat{\sigma}_{K'}t} - e^{i\hat{\sigma}_K t}}{(\sigma_K + \sigma_{K'}) (\hat{\sigma}_K - \hat{\sigma}_{K'})} \times \left(1 + \frac{2(\hat{\sigma}_K \delta\sigma_K - \hat{\sigma}_{K'} \delta\sigma_{K'})}{(\sigma_K + \sigma_{K'}) (\hat{\sigma}_K - \hat{\sigma}_{K'})} \right) \times \sum_{\substack{k \in K \\ k' \in K'}} \langle R|u_k \rangle \langle v_k | \delta A | u_{k'} \rangle \langle v_{k'} | S \rangle \right\}. \quad (\text{A.14})$$

We now consider the non-linearized PAVA seismogram defined as:

$$s_1 = \sum_K e^{i\hat{\sigma}_K t} A_K(0), \quad (\text{A.15})$$

which can be approximated up to the second order in $O(\delta\sigma_K t)$ as:

$$\begin{aligned} & \sum_K e^{i\hat{\sigma}_K t} A_K(0) \\ & \simeq \sum_K e^{i\sigma_K t} A_K(0) \left(1 + i\delta\sigma_K t - \frac{1}{2} \delta\sigma_K^2 t^2 \right) \\ & = \sum_K e^{i\sigma_K t} A_K(0) + \sum_K i\delta\sigma_K t e^{i\sigma_K t} A_K(0) \\ & \times (1 + i\delta\sigma_K t) + \sum_K \frac{1}{2} \delta\sigma_K^2 t^2 e^{i\sigma_K t} A_K(0). \end{aligned} \quad (\text{A.16})$$

Using the first-order approximation in $O(\delta\sigma_K t)$: $1 + i\delta\sigma_K t \simeq e^{i\delta\sigma_K t}$, the reference seismogram (spherical earth) can be written:

$$\begin{aligned} s_0(t) & = \sum_K e^{i\sigma_K t} A_K(0) \\ & \simeq \sum_K e^{i\hat{\sigma}_K t} A_K(0) - \sum_K i\delta\sigma_K t e^{i\hat{\sigma}_K t} A_K(0) \\ & \quad - \sum_K \frac{1}{2} \delta\sigma_K^2 t^2 e^{i\sigma_K t} A_K(0). \end{aligned} \quad (\text{A.17})$$

Finally, using Eqs. (A.14) and (A.17), and keeping the first-order terms in $O(\delta\sigma_K t)$, we obtain the following expression for the seismogram:

$$\begin{aligned} s(t) & = \sum_K A_K(0) e^{i\hat{\sigma}_K t} - \sum_K i\delta\sigma_K t A_K(0) e^{i\hat{\sigma}_K t} \\ & \quad \times \sum_{K' \in \Gamma_K} \left\{ \frac{e^{i\hat{\sigma}_K t} - e^{i\hat{\sigma}_{K'} t}}{(\sigma_K + \sigma_{K'}) (\hat{\sigma}_K - \hat{\sigma}_{K'})} \right. \\ & \quad \left. \times \sum_{\substack{k \in K \\ k' \in K'}} \langle R|u_k \rangle \langle v_k | \delta A | u_{k'} \rangle \langle v_{k'} | S \rangle \right\}. \end{aligned} \quad (\text{A.18})$$

This equation is equivalent to the NACT expression given by Li and Romanowicz (1995).

References

- Alsina, D., Snieder, R., 1996. constraint on the velocity structure beneath the Tornquist–Tesseyre zone from beam forming analysis. *Geophys. J. Int.* 126, 205–218.
- Alsina, D., Woodward, R.L., Snieder, R., 1996. Shear wave velocity structure in North America from large-scale waveform inversion of surface waves. *J. Geophys. Res.* 101, 15969–15986.
- Clévéde, E., Lognonné, P., 1996a. Fréchet derivatives of coupled seismograms with respect to an anelastic rotating Earth. *Geophys. J. Int.* 124, 456–482.
- Clévéde, E., Lognonné, P., 1996b. Corrigendum to Fréchet derivatives of coupled seismograms with respect to an anelastic rotating Earth. *Geophys. J. Int.* 126, 903.
- Cummins, P.R., Takeuchi, N., Geller, R.J., 1997. Computation of complete synthetic seismograms for laterally heterogeneous models using the Direct Solution Method. *Geophys. J. Int.* 130, 1–16.

- Dahlen, F.A., 1987. Multiplet coupling and the calculation of synthetic seismograms. *Geophys. J.R. Astron. Soc.* 91, 241–254.
- Dziewonski, A.M., 1995. Global seismic tomography of the mantle. *Rev. Geophys.* 33, 419–423, Supplement.
- Dziewonski, A.M., Anderson, D.L., 1981. Preliminary reference Earth model. *Phys. Earth Planet. Inter.* 25, 297–356.
- Edmonds, A.R., 1960. *Angular Momentum and Quantum Mechanics*. Princeton Univ. Press, NJ.
- Friederich, W., 1998. Wave-theoretical inversion of teleseismic surface waves in a regional network: phase velocity maps and a three-dimensional upper mantle shear wave velocity model for southern Germany. *Geophys. J. Int.* 132, 203–225.
- Friederich, W., Wielandt, E., Stange, S., 1993. Multiple forward scattering of surface waves — comparison with an exact solution and Born single-scattering methods. *Geophys. J. Int.* 112, 264–275.
- Geller, R.J., Hara, T., 1993. Two efficient algorithms for iterative linearized inversion of seismic waveform data. *Geophys. J. Int.* 115, 699–710.
- Geller, R.J., Hara, T., Tsuboi, S., 1990. On the equivalence of two methods for computing partial derivatives of seismic waveform. *Geophys. J. Int.* 100, 153–156.
- Hara, T., Tsuboi, S., Geller, R.J., 1993. Inversion for laterally heterogeneous upper mantle S-wave velocity structure using iterative waveform inversion. *Geophys. J. Int.* 115, 667–698.
- Jordan, T.H., 1978. A procedure for estimating lateral variations from low-frequency eigenspectra data. *Geophys. J.R. Astron. Soc.* 52, 441–455.
- Li, X.-D., Romanowicz, B., 1995. Comparison of global waveform inversions with and without considering cross-branch modal coupling. *Geophys. J. Int.* 121, 695–709.
- Li, X.-D., Romanowicz, B., 1996. Global mantle shear velocity model developed using non-linear asymptotic coupling theory. *J. Geophys. Res.* 101, 22245–22272.
- Li, X.-D., Tanimoto, T., 1993. Waveforms of long-period body waves in a slightly aspherical Earth model. *Geophys. J. Int.* 112, 92–102.
- Lognonné, P., 1991. Normal modes and seismograms of an anelastic rotating Earth. *J. Geophys. Res.* 96, 20309–20319.
- Lognonné, P., Clévéde, E., 1997. Diffraction of long-period Rayleigh waves by a slab: effects of mode coupling. *Geophys. Res. Lett.* 24, 1035–1038.
- Lognonné, P., Romanowicz, B., 1990. Modelling of coupled normal modes of the Earth: the spectral method. *Geophys. J. Int.* 102, 365–395.
- Mégnin, C., Bunge, H.-P., Romanowicz, B., Richards, M.A., 1997. Imaging 3-D spherical convection models, what can seismic tomography tell us about mantle dynamics? *Geophys. Res. Lett.* 24, 1299–1303.
- Mégnin, C., Romanowicz, B., 1999a. The effects of theoretical formalism and data selection on mantle models derived from waveform tomography. *Geophys. J. Int.* 138, 366–380.
- Mégnin, C., Romanowicz, B., 1999. A comparison between tomographic and geodynamic models of the Earth's mantle, History and dynamics of plate motions, AGU monograph, in press.
- Meier, T., Lebedev, S., Nolet, G., Dahlen, F.A., 1997a. Diffraction tomography using multimode surface waves. *J. Geophys. Res.* 102, 8255–8267.
- Meier, T., Malischewski, P.G., Neunhöfer, H., 1997b. Reflection and transmission of surface waves at a vertical discontinuity and imaging of lateral heterogeneity using reflected fundamental Rayleigh waves. *Bull. Seismol. Soc. Am.* 87, 1648–1661.
- Pollitz, F., 1994. Surface wave scattering from sharp lateral discontinuities. *J. Geophys. Res.* 99, 21891–21909.
- Park, J., 1987. Asymptotic coupled-mode expressions for multiplet amplitude anomalies and frequency shifts on an aspherical Earth. *Geophys. J.R. Astron. Soc.* 90, 129–169.
- Park, J., 1989. Roughness constraints in surface wave tomography. *Geophys. Res. Lett.* 16, 1329–1332.
- Park, J., 1990. The subspace projection method for constructing first-order coupled-mode long-period synthetic seismograms. *Geophys. J. Int.* 101, 111–124.
- Press, W.H., Teukolsky, S.A., Vetterling, W.T., Flannery, B.P., 1992. *Numerical Recipes in C*, 2nd edn. Cambridge Univ. Press.
- Ritzwoller, M.H., Lavelly, E.M., 1995. Three-dimensional seismic models of the Earth's mantle. *Rev. Geophys.* 33, 1–66.
- Romanowicz, B., 1987. Multiplet–multiplet coupling due to lateral heterogeneity: asymptotic effects on the amplitude and frequency of the Earth's normal modes. *Geophys. J.R. Astron. Soc.* 90, 75–100.
- Romanowicz, B., Roul, G., 1986. First-order asymptotics for the eigenfrequencies of the Earth and application to the retrieval of large-scale variations of structure. *Geophys. J.R. Astron. Soc.* 87, 209–239.
- Snieder, R., Nolet, G., 1987. Linearized scattering of surface waves on a spherical Earth. *J. Geophys.* 61, 55–63.
- Snieder, R., Romanowicz, B., 1988. A new formalism for the effect of lateral heterogeneity on normal modes and surface waves: I. Isotropic perturbations, perturbations of interfaces and gravitational perturbations. *Geophys. J.R. Astron. Soc.* 92, 207–221.
- Suetsugu, D., Nakanishi, I., 1985. Tomographic inversion and resolution for Rayleigh wave phase velocities in the Pacific Ocean. *J. Phys. Earth* 33, 345–368.
- Tanimoto, T., 1984. A simple derivation of the formula to calculate synthetic long-period seismograms in a heterogeneous Earth by normal mode summation. *Geophys. J.R. Astron. Soc.* 77, 275–278.
- Tromp, J., Dahlen, F.A., 1992. Variational principles for surface wave propagation on a laterally heterogeneous Earth: 2. Frequency domain JWKB theory. *Geophys. J. Int.* 109, 599–619.
- Tromp, J., Dahlen, F.A., 1993. Maslov theory for surface wave propagation on a laterally heterogeneous Earth. *Geophys. J. Int.* 115, 512–528.
- Um, J., Dahlen, F.A., Park, J., 1991. Normal mode multiplet coupling along a dispersion branch. *Geophys. J. Int.* 106, 11–35.
- Wang, Z., Dahlen, F.A., 1994. JWKB surface-wave seismograms on a laterally heterogeneous Earth. *Geophys. J. Int.* 119, 381–401.
- Woodhouse, J.H., 1980. The coupling and attenuation of nearly

- resonant multiplets in the Earth's free oscillation spectrum. *Geophys. J.R. Astron. Soc.* 61, 261–283.
- Woodhouse, J.H., 1983. The joint inversion of seismic wave forms for lateral variations in Earth structure and earthquake source parameters. In: Kanamori, H., Boschi, E. (Eds.), *Earthquakes: Observations, Theory and Interpretation*. Proc. Int. School Phys. Enrico Fermi, LXXXV, pp. 366–397.
- Woodhouse, J.H., Dziewonski, A.M., 1984. Mapping the upper mantle: three-dimensional modeling of the Earth structure by inversion of seismic waveforms. *J. Geophys. Res.* 89, 5953–5986.
- Woodhouse, J.H., Girnius, T.P., 1982. Surface waves and free oscillations in a regionalized Earth model. *Geophys. J.R. Astron. Soc.* 68, 653–673.
- Woodhouse, J.H., Wong, Y.K., 1986. Amplitude, phase and path anomalies of mantle waves. *Geophys. J.R. Astron. Soc.* 87, 753–773.